Supporting Information

Multifunctional Electrocatalysis on Transition Metal-Doped Biphenylene: A First-Principles and Machine Learning Study of Single-Atom Catalysts for HER, OER, and ORR

Dinesh Kumar Dhanthala Chittibabu and Hsin-Tsung Chen*

Department of Chemistry, R&D Center for Membrane Technology, and Research Center for Semiconductor Materials and Advanced Optics, Chung Yuan Christian University, Chungli District, Taoyuan City 320314, Taiwan.

Corresponding author. E-mail: htchen@cycu.edu.tw; Tel: +886-3-265-3324

The structural coordinate of BPN

BPN

1.00000000000000

7.5133489999999998 0.0000000000000000 0.0000000000000000

-0.0011234000000000 9.0516399300000003 0.0000000000000000

0.0143286800000000 0.0160580500000000 19.9604284000000014

C

24

Selective dynamics

Direct

0.5967207624407623	0.8306180558724151	0.5000224583518282	T	T	T
0.5966806333479446	0.6693615094442255	0.5000196477089651	T	T	T
0.7500452728673489	0.5800251701405523	0.5002607635066915	T	T	T
0.9033791687634937	0.6693749917955737	0.4999847472391314	T	T	T
0.9034118986258006	0.8306367358610756	0.4999792376160390	T	T	T
0.7500678171273203	0.9199899781506848	0.5002602477606130	T	T	T
0.4033727150938162	0.8306552510833713	0.4996266656760698	T	T	T
0.4033332389508978	0.6693627625312532	0.4996326052451633	T	T	T
0.2500326223242448	0.5799404226995468	0.4994943311410112	T	T	T
0.0967313653164151	0.6693482248841199	0.4995942291782372	T	T	T
0.0967630533500303	0.8306342584709557	0.4995944066992428	T	T	T
0.2500592544279960	0.9200478290728671	0.4994926357557603	T	T	T
0.5966667610500613	0.3306372374696421	0.5003673942538472	T	T	T
0.5966272843301539	0.1693447493521629	0.5003743343024624	T	T	T
0.7499407449959812	0.0799521713626674	0.5005083642227789	T	T	T
0.9032369453190096	0.1693657415290443	0.5004055933007572	T	T	T
0.9032686335022795	0.3306527760394766	0.5004057708217629	T	T	T
0.7499673776757552	0.4200595773004531	0.5005056688589886	T	T	T
0.4033193653210952	0.3306384905557741	0.4999803522910352	T	T	T
0.4032792362282773	0.1693819441275848	0.4999775416481717	T	T	T
0.2499321821179057	0.0800100225185540	0.4997387522608550	T	T	T
0.0965891009284590	0.1693632641389242	0.5000207623839609	T	T	T
0.0966208312365065	0.3306250082044265	0.5000152527608688	T	T	T
0.2499547271326509	0.4199748298594477	0.4997392364933086	T	T	T

Note S1. Computational Details

The formula for calculating the Gibbs free energy (G) of each intermediate of HER/OER/ORR by computational hydrogen electrode (CHE) model proposed by Nørskov et al.[1] The chemical potential of the $H^+ + e^-$ pair in aqueous solution is related to that of half of the H_2 gas molecule at standard hydrogen electrode (SHE) conditions. According to this method, the G value can be determined as follows:

$$\Delta G = \Delta E + \Delta E_{ZPE} - T\Delta S + \Delta G_U + \Delta G_{pH} \quad \text{(S1)}$$

In this equation, ΔE is the adsorption energies of the intermediate. ΔE_{ZPE} is the zero-point energy correction, T is the temperature (set to 298.15 K), and ΔS is the entropy change. The entropies of gas-phase molecules are looked up in the NIST database,[2] and the post-processing of energy corrections (zero-point energy and entropy) for adsorbed species were performed with the help of VASPKIT code.[3] ΔG_U is the free energy contribution related to applied potential U, which can be determined as $\Delta G_U = -eU$, where e and U represent the number of transferred electrons and applied electrode potential. ΔG_{pH} is the correction of H^+ free energy with concentration,

$$\Delta G_{pH} = K_B T \times \ln 10 \times pH \quad \text{(S2)}$$

K_B represents the Boltzmann constant.

The U value is determined by the equation

$$U = -\Delta G_{max}/e \quad \text{(S3)}$$

where ΔG_{max} is free energy change in potential-determining step. According to the CHE model, U and pH are 0.

Note S2. HER:

The HER process involves two proton-coupled electron transfer, and in the acid solution the 2-electron transfer pathways can be written as the equation S4-S6:

$$* + H+ + e^- \rightarrow *H \text{ (Volmer)} \quad \text{(S4)}$$

$$*H + H+ + e^- \rightarrow * + H_2(g) \text{ (Heyrovsky)} \quad \text{(S5)}$$

Or

$$*H + *H \rightarrow * + H_2(g) \text{ (Tafel)} \quad \text{(S6)}$$

The * represents a free adsorption site. The free energy diagram for the overall HER process is normally a three-state one, comprising by an initial-state ($H^+ + e^-$), an intermediate-state of H adsorbed on the catalyst surface (*H), and a final-state product represented by $\frac{1}{2}H_2$. [4] In the present study, extra states of $*H_2$ or 2*H adsorption were also considered to take Heyrovsky or Tafel steps into consideration. Tafel Pathway which is chemical recombination between two surface hydrogen atoms, more efficient route but requires facile surface diffusion so the atoms can discover one another at the recombination site. The best HER catalysts feature low barriers for surface hydrogen diffusion and can therefore take advantage of the kinetically preferred chemical (Tafel) recombination mechanism.[5, 6] On TM@SV–BPN, surface hydrogen diffusion between active sites requires transfer of the hydrogen substrate between the TM atom and carbon matrix and is likely to be prohibitively slow. This renders a kinetically efficient Tafel mechanism for HER improbable. We choose best two catalysts (Mo@SV–BPN and Tc@SV–BPN) to study Tafel route. we find that there exists a secondary intermediate state between TM-bound surface atomic hydrogen and the free gaseous H_2 molecule. This intermediate is based on a Kubas interaction,[7, 8] in which the H_2 molecule is associated yet chemisorbed (see below Figure). If binding is sufficiently strong, the Kubas complex can reduce the kinetic barrier involved in bond breaking and subsequent bond reformation and introduce a modified Kubas-mediated HER pathway with enhanced efficiency. The first step involves proton abstraction onto the TM, as usual. However, the next step involves binding of a second hydrogen atom directly into the Kubas complex, which subsequently desorbs as molecular H_2. Note that this process has beneficial aspects in common with both the Tafel and the Heyrovsky mechanisms, in that it involves the chemical association of two surface-bound hydrogen atoms (like the Tafel mechanism), yet does not require surface diffusion because the process can happen fully on the TM site (like the Heyrovsky mechanism).

The HER catalytic activity was depicted via calculating the reaction Gibbs free energy of hydrogen adsorption (ΔG_{*H}) based on the equation (S7)

$$\Delta G_{*H} = \Delta E_{*H} + \Delta E_{ZPE} - T\Delta S_{*H} \quad (S7)$$

where ΔE_{*H} is the hydrogen adsorption energy, ΔE_{ZPE} refers to the zero-point energy between the gas-phase hydrogen and adsorbed hydrogen and ΔS_{*H} is the entropy difference between gas phase and adsorbed hydrogen. T indicates the room temperature of 298.15 K. Both ΔE_{ZPE} and $T\Delta S_{*H}$ can be obtained from the calculations of vibrational frequencies.

The theoretical overpotential for HER is defined as

$$\eta^{HER} = |\Delta G_{*H}|/e \quad (S8)$$

Where G_{*H} is the change of Gibbs free energy for hydrogen adsorption. Standard conditions (pH = 0, T = 298.15 K) and applied potential U = 0 V vs SHE. A smaller η^{HER} indicates a higher activity of the electrocatalyst.

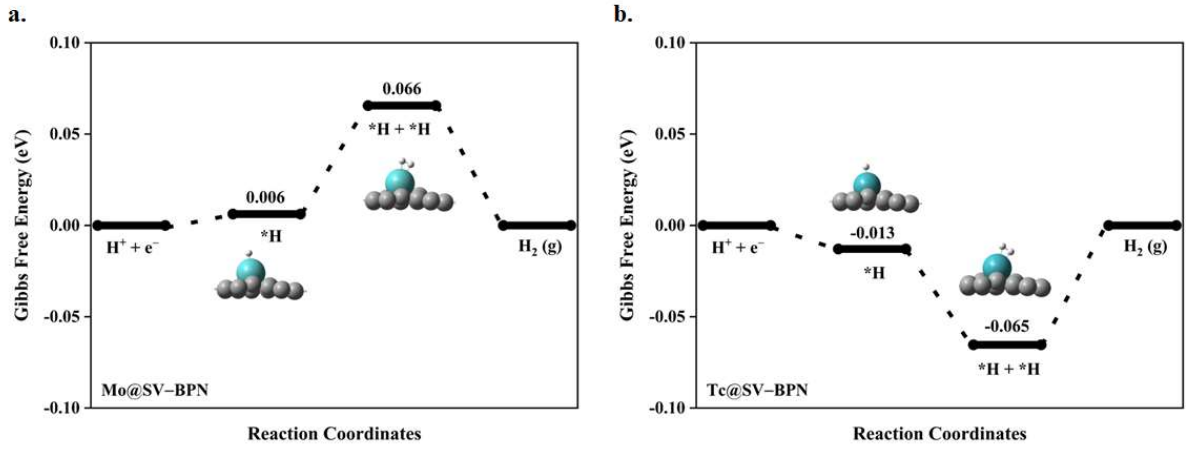

Figure for the Volmer-Kubas reaction pathway of Mo@SV–BPN and Tc@SV–BPN.

Note S3. The theoretical exchange current i_0:

The theoretical exchange current i_0 was calculated using equation.

$$i_0 = -ek_0 \frac{1}{1+exp(|\Delta G*_H|/k_bT)} \quad \text{(S9)}$$

Where k_0 is the rate constant. As there is no experimental data available, k_0 is set to 1. k_B is the Boltzmann constant (K_B= 1.380 649 × 10^{-}23 J K^{-1}) and T is the temperature (T=298.15 K).

Note S4. OER

The overall reaction of OER in an acidic environment (pH = 0) can be described as.[9]

$$2H_2O\ (l) \rightarrow O_2\ (g) + 4H^+ + 4e^- \quad \text{(S10)}$$

The following are the four-electron reaction steps for OER processes:

$$H_2O\ (l) + * \rightarrow *OH + H^+ + e^- \quad \text{(S11)}$$

$$*OH \rightarrow *O + H^+ + e^- \quad \text{(S12)}$$

$$H_2O\ (l) + *O \rightarrow *OOH + H^+ + e^- \quad \text{or} \quad H_2O\ (l) + *O \rightarrow *O*OH + H^+ + e^- \quad \text{(S13)}$$

$$*OOH \rightarrow O_2\ (g) + * + H^+ + e^- \quad \text{(S14)}$$

Where * refers to the catalyst and active adsorption site on the catalyst; (l) and (g) represent the liquid and gas phases, respectively; and *OH, *O, and *OOH represent the corresponding adsorbed intermediates.

Note S5. ORR

ORR in the acidic environment could be expressed as[10]

$$O_2\,(g) + 4H^+ + 4e^- \rightarrow 2H_2O\ \ (l) \tag{S15}$$

The concrete ORR steps in the acidic environment experience two possible reaction mechanisms, namely associative and dissociative processes. For the associative process, the adsorbed $*O_2$ is firstly hydrogenated to form the *OOH, ORR can be regarded as a reverse reaction of OER, which occurs at the cathode of the fuel cells and air batteries.

$$*O_2 + H^+ + e^- \rightarrow *OOH \tag{S16}$$

$$*OOH + H^+ + e^- \rightarrow *O + H_2O\ (l) \tag{S17}$$

$$*O + H^+ + e^- \rightarrow *OH \tag{S18}$$

$$*OH + H^+ + e^- \rightarrow * + H_2O\ (l) \tag{S19}$$

While for the associative process, the adsorbed $*O_2$ first decomposes into two *O, and then every *O will gradually form H_2O molecules by hydrogenation.

$$*O_2 \rightarrow 2*O \tag{S20}$$

$$2*O + H^+ + e^- \rightarrow *OH + *O \tag{S21}$$

$$*OH + *O + H^+ + e^- \rightarrow *O + H_2O\ (l) \quad (S22)$$

$$*O + H^+ + e^- \rightarrow *OH \quad (S23)$$

$$*OH + H^+ + e^- \rightarrow * + H_2O\ (l) \quad (S24)$$

During the two-electron pathway, ORR in the acidic environment could be expressed as

$$O_2 + 2H^+ + 2e^- \rightarrow H_2O_2 \quad (S25)$$

Note S6. Adsorption energy calculations for OER/ORR

These adsorption energies of intermediates can be calculated according to equation (S26) - (S29):

$$\Delta G_{*OH} = G_{*OH} - G_{*} - G_{H2O} + 1/2G_{H2} \quad (S26)$$

$$\Delta G_{*O} = G_{*O} - G_{*} - G_{H2O} + G_{H2} \quad (S27)$$

$$\Delta G_{*OOH} = G_{*OOH} - G_{*} - 2G_{H2O} + 3/2G_{H2} \quad (S28)$$

$$\Delta G_{*O*OH} = G_{*O*OH} - G_{*} - 2G_{H2O} + 3/2G_{H2} \quad (S29)$$

Where GG_{*OH}, G_{*O} and G_{*OOH} are the Gibbs free energies of *OH, *O and *OOH, H_2O and H_2, respectively. To calculate the Gibbs reaction free energy change (ΔG) for each individual step, the experimental reaction energy of equation 4.92 eV is taken into consideration to calculate the free energy of O_2 gas. The energy of the ($H^+ + e^-$) pair can be replaced by half of the H_2 molecule at 298.15 K.

The Gibbs free energy change can be written as

$$\Delta G_1 = \Delta G_{*OH} \quad (S30)$$

$$\Delta G_2 = \Delta G_{*O} - \Delta G_{*OH} \quad (S31)$$

$$\Delta G_3 = \Delta G_{*OOH} - \Delta G_{*O} \quad (S32)$$

$$\Delta G_4 = 4.92 - \Delta G_{*OOH} \quad (S33)$$

ORR is reversible pathway of OER, hence the four e^- pathway can be obtained as

$$\Delta G_5 = -\Delta G_4 \quad (S34)$$

$$\Delta G_6 = -\Delta G_3 \quad \text{(S35)}$$

$$\Delta G_7 = -\Delta G_2 \quad \text{(S36)}$$

$$\Delta G_8 = -\Delta G_1 \quad \text{(S37)}$$

The overpotential for the OER and ORR pathways can be obtained using the relation.

Note S7. Theoretical Overpotential Calculation for OER/ORR

The theoretical overpotential of OER (η^{OER}) is used to assess the activity of the catalysts, which is obtained by

$$\eta^{OER} = \max\{G_1, G_2, G_3, \text{and } G_4\}/e - 1.23 \quad \text{(S38)}$$

Since the ORR and OER are inverse reactions to each other, the overpotential of the ORR (η^{ORR}) can be expressed as

$$\eta^{ORR} = \max\{G_5, G_6, G_7, \text{and } G_8\}/e + 1.23 \quad \text{(S39)}$$

Lower the overpotential better catalytic activity.

Note S8. d-band Center

The value of the d-band center of the embedded single metal atoms on @SV–BPN can be calculated by using the following equation

$$\varepsilon_d = \frac{\int_{-\infty}^{\infty} \varepsilon \rho_d d\varepsilon}{\int_{-\infty}^{\infty} \rho_d d\varepsilon} \quad \text{(S40)}$$

Where ρ_d and ε are the projected density of states of d orbital of TM atoms and the energy width of the TM-d orbitals, respectively.

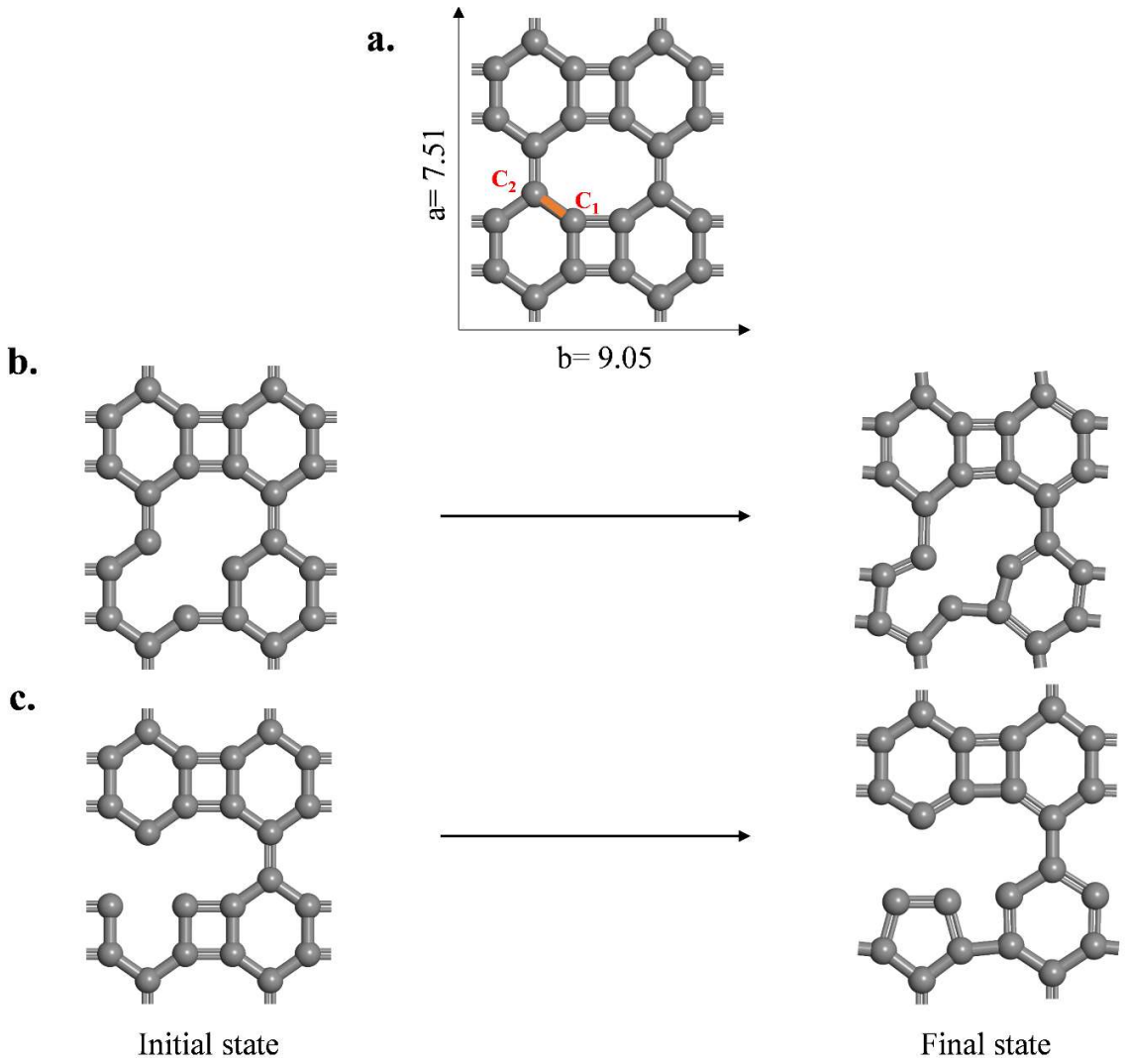

Figure S1. a) 2 ×2 optimized biphenylene. b) before and after optimized single vacancy of C_1 and c) C_2.

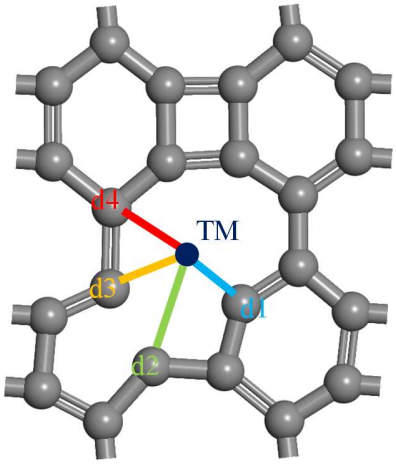

Figure S2. C_1 defective biphenylene, d1, d2, d3 and d4 represents distance between transition mental and carbon atoms.

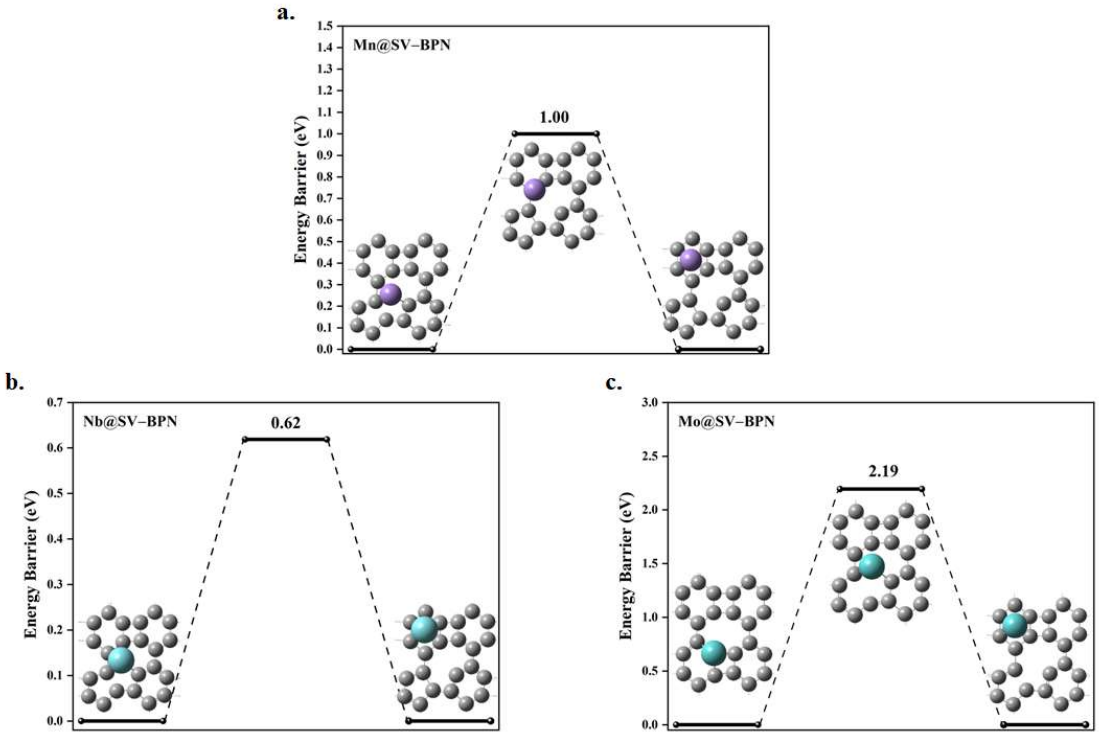

Figure S3. The calculated diffusion barriers for (a) Mn, (b) Nb and (c) Mo migration on the SV–BPN substrate.

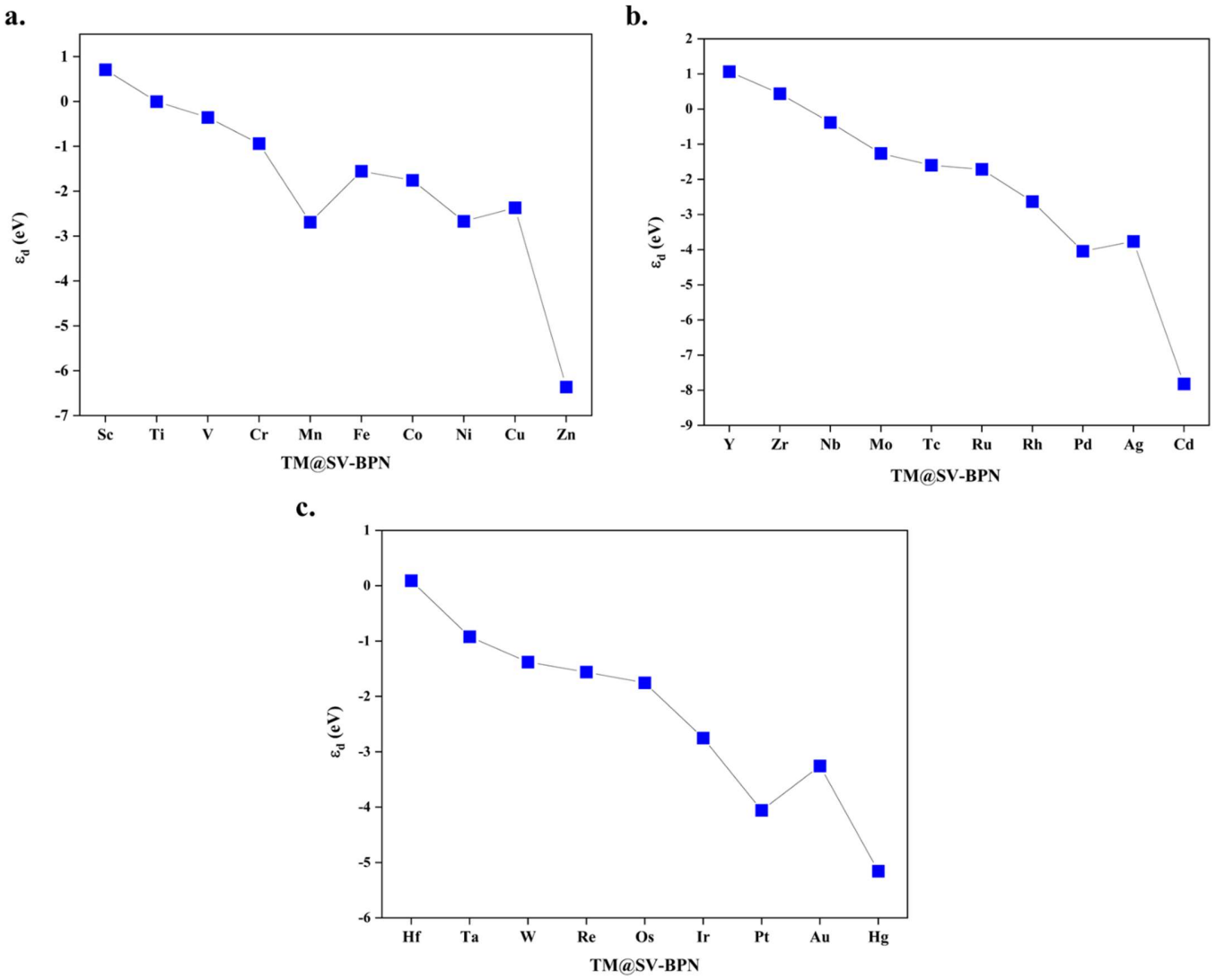

Figure S4. The ε_d of (a) 3d TM, (b) 4d TM and (c) 5d TM.

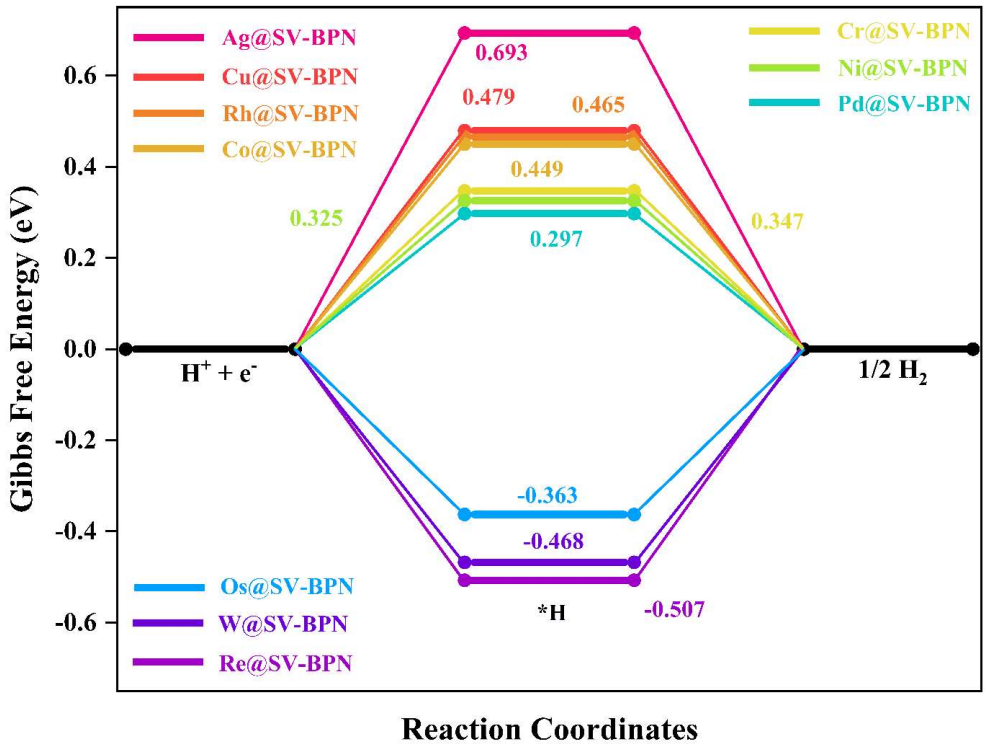

Figure S5. Gibbs free energy diagram of HER.

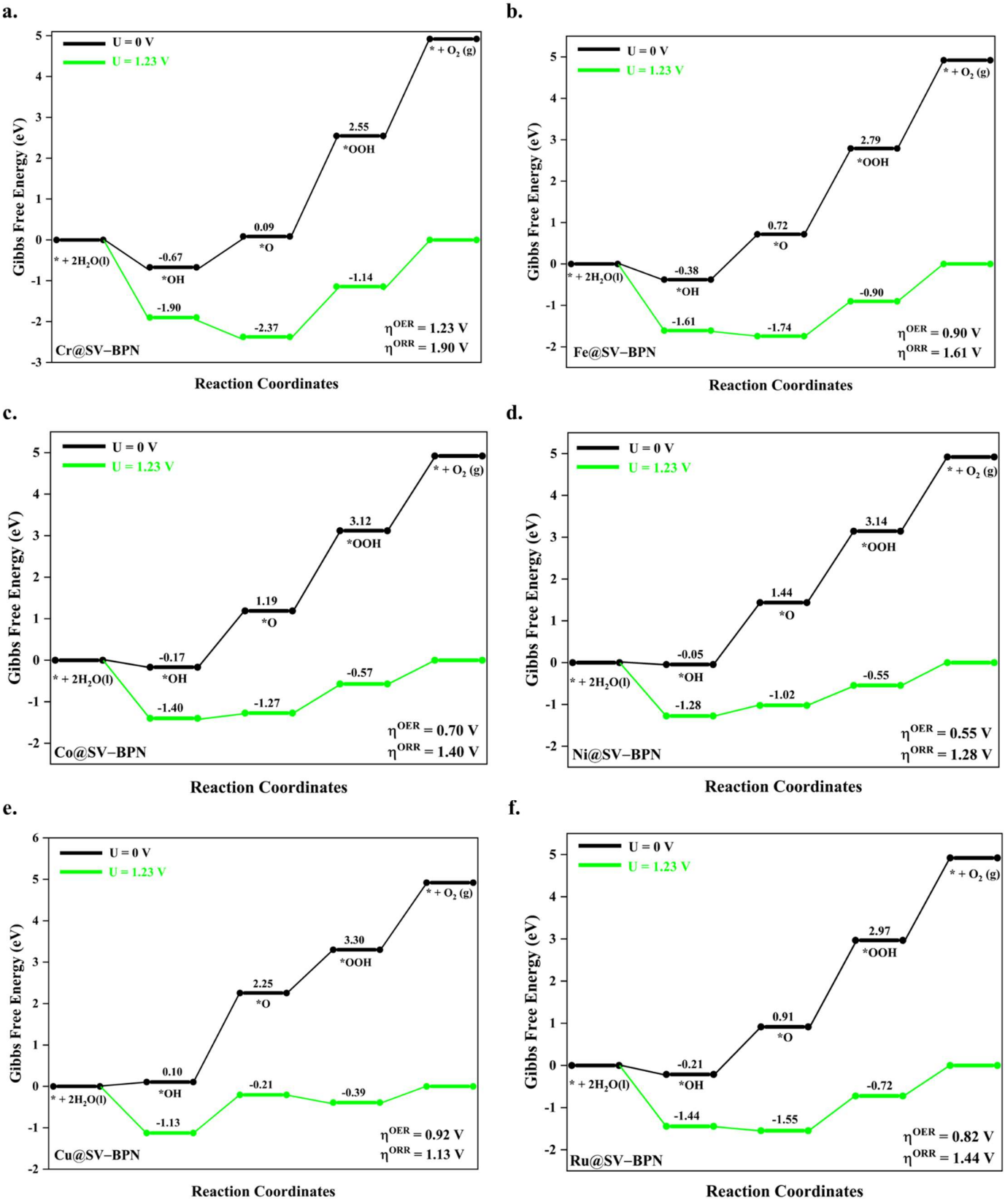
a.
U = 0 V
U = 1.23 V
Gibbs Free Energy (eV)
* + 2H2O(l)
-0.67
*OH
0.09
*O
2.55
*OOH
* + O2 (g)
-1.90
-2.37
-1.14
η^OER = 1.23 V
η^ORR = 1.90 V
Cr@SV–BPN
Reaction Coordinates
b.
U = 0 V
U = 1.23 V
Gibbs Free Energy (eV)
* + 2H2O(l)
-0.38
*OH
0.72
*O
2.79
*OOH
* + O2 (g)
-1.61
-1.74
-0.90
η^OER = 0.90 V
η^ORR = 1.61 V
Fe@SV–BPN
Reaction Coordinates
c.
U = 0 V
U = 1.23 V
Gibbs Free Energy (eV)
* + 2H2O(l)
-0.17
*OH
1.19
*O
3.12
*OOH
* + O2 (g)
-1.40
-1.27
-0.57
η^OER = 0.70 V
η^ORR = 1.40 V
Co@SV–BPN
Reaction Coordinates
d.
U = 0 V
U = 1.23 V
Gibbs Free Energy (eV)
* + 2H2O(l)
-0.05
*OH
1.44
*O
3.14
*OOH
* + O2 (g)
-1.28
-1.02
-0.55
η^OER = 0.55 V
η^ORR = 1.28 V
Ni@SV–BPN
Reaction Coordinates
e.
U = 0 V
U = 1.23 V
Gibbs Free Energy (eV)
* + 2H2O(l)
0.10
*OH
2.25
*O
3.30
*OOH
* + O2 (g)
-1.13
-0.21
-0.39
η^OER = 0.92 V
η^ORR = 1.13 V
Cu@SV–BPN
Reaction Coordinates
f.
U = 0 V
U = 1.23 V
Gibbs Free Energy (eV)
* + 2H2O(l)
-0.21
*OH
0.91
*O
2.97
*OOH
* + O2 (g)
-1.44
-1.55
-0.72
η^OER = 0.82 V
η^ORR = 1.44 V
Ru@SV–BPN
Reaction Coordinates

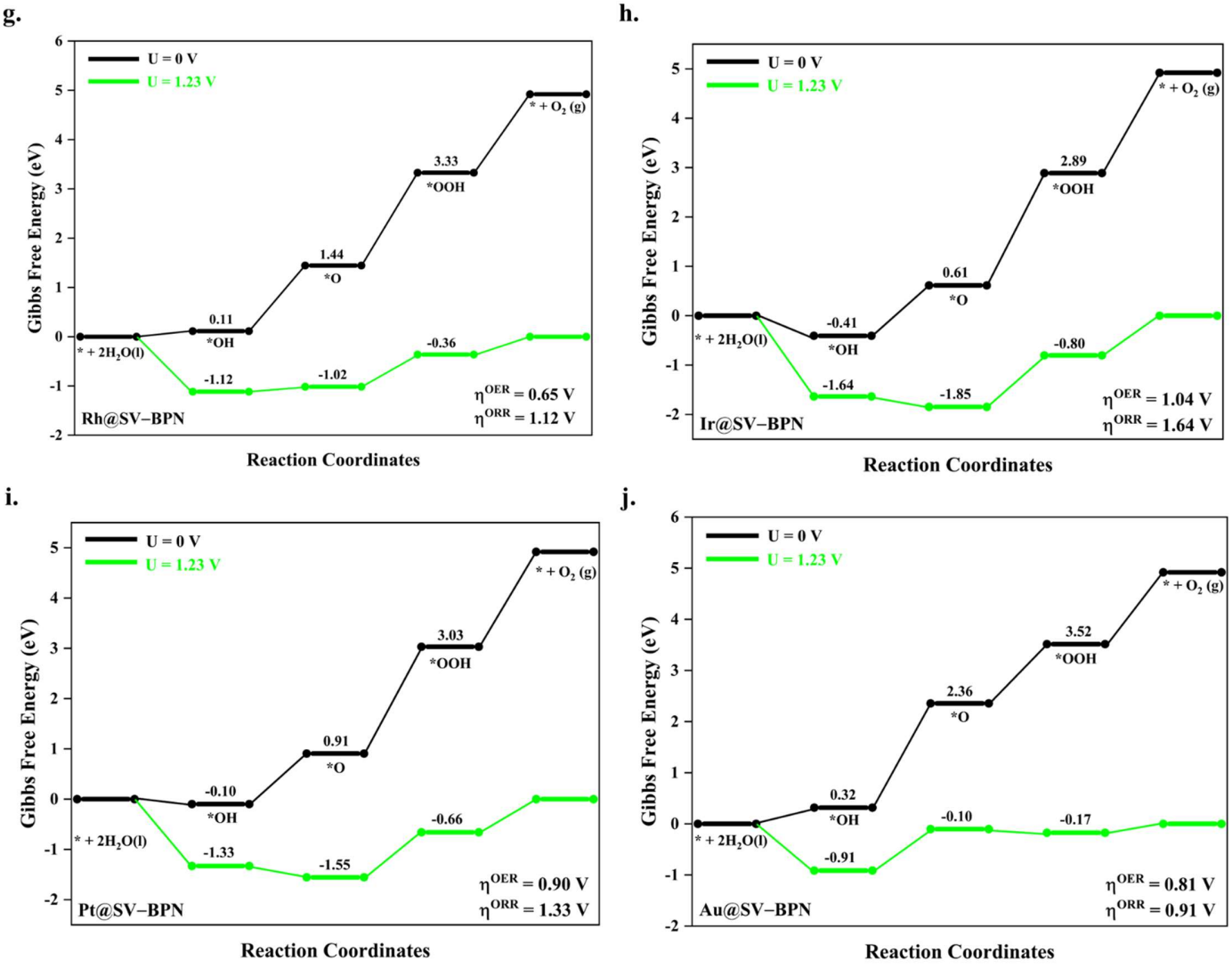

Figure S6. The Gibbs free energy diagram of OER/ORR reaction on TM@SV–BPN catalysts. The OER reaction is the counter-clock wise, and the reverse direction refers to the ORR. (a) Cr, (b) Fe, (c) Co, (d) Ni, (e) Cu, (f) Ru, (g) Rh, (h) Ir, (i) Pt, and (j) Au@SV–BPN.

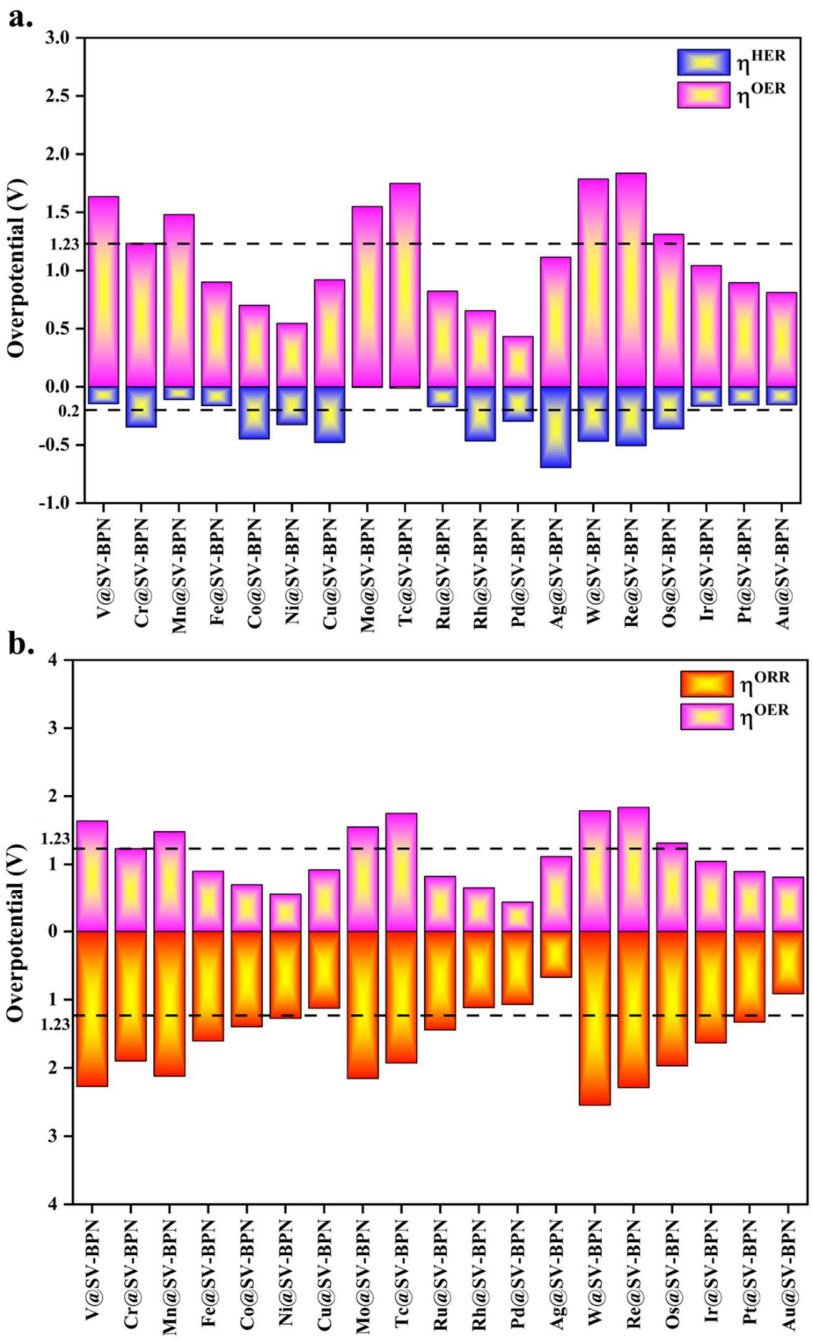

Figure S7. (a) Bifunctional overpotential for water-splitting (η^{HER}/η^{OER}) and (b) bifunctional overpotential for metal-air batteries (η^{OER}/η^{ORR}).

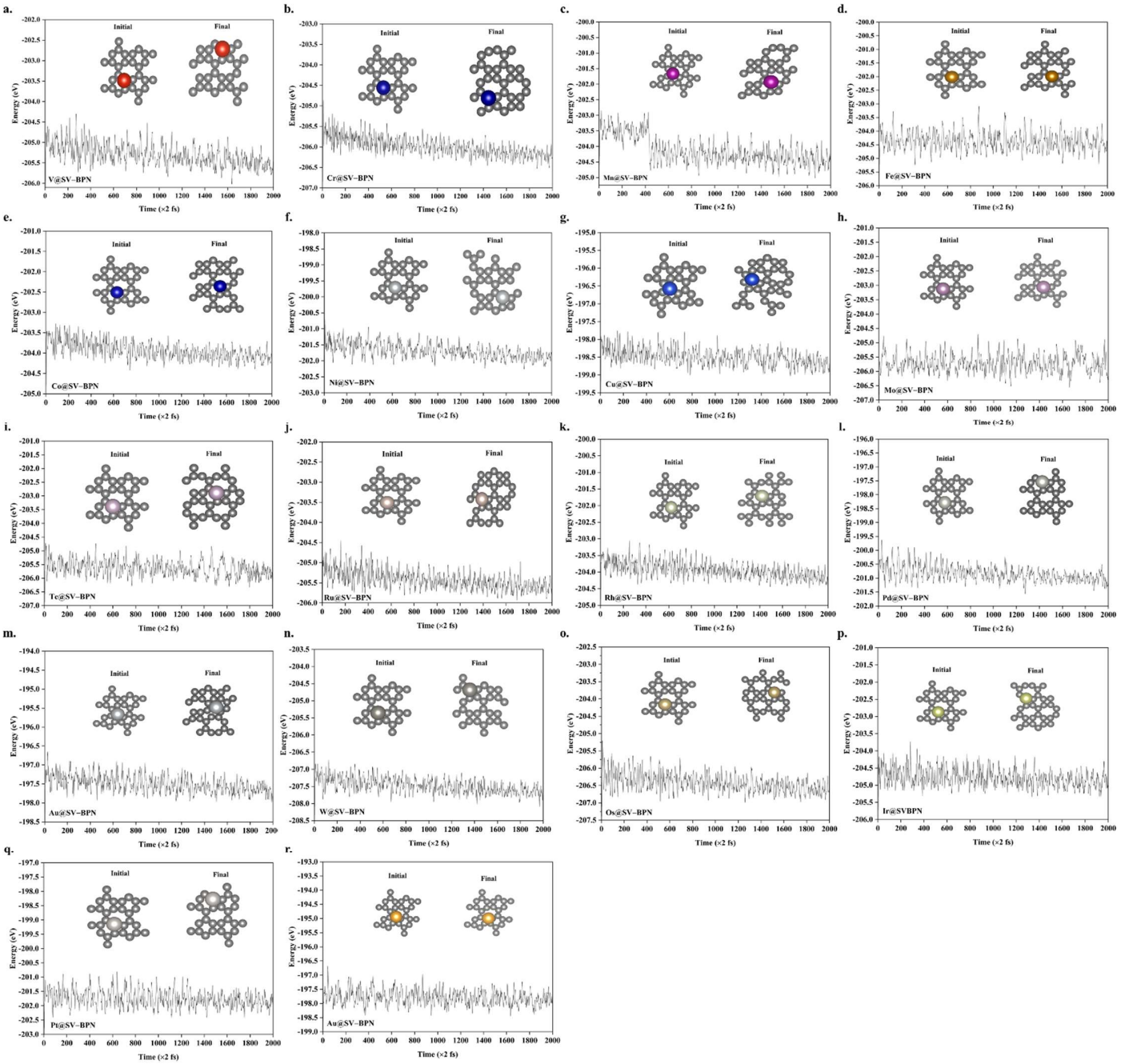

Figure S8. AIMD simulations at temperature of 500 K with 4 ps time step for duration of 2 fs for TM@SV–BPN catalysts. (a) V, (b) Cr, (c) Mn, (d) Fe, (e) Co, (f) Ni, (g) Cu, (h) Mo, (i) Tc, (j) Ru, (k) Rh, (l) Pd, (m) Au, (n) W, (o) Os, (p) Ir, (q) Pt and (r) Au@SV–BPN.

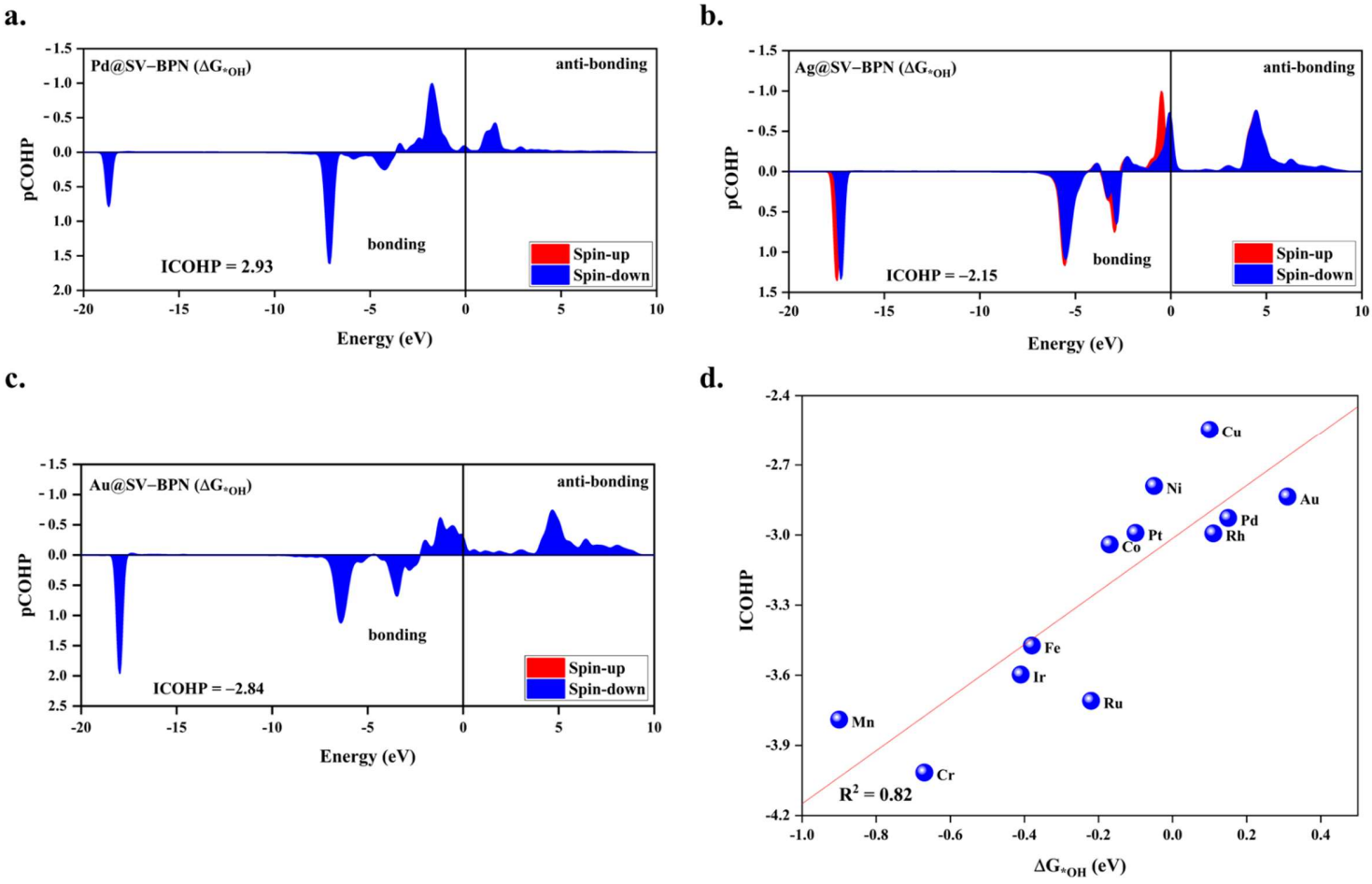

Figure S9. pCOHP of (a) Pd@SV–BPN, (b) Ag@SV–BPN, and (c) Au@SV–BPN with reaction intermediate *OH, where the fermi level set to zero. ICOHP. (d) The relationship between ΔG_{*OH} and ICOHP.

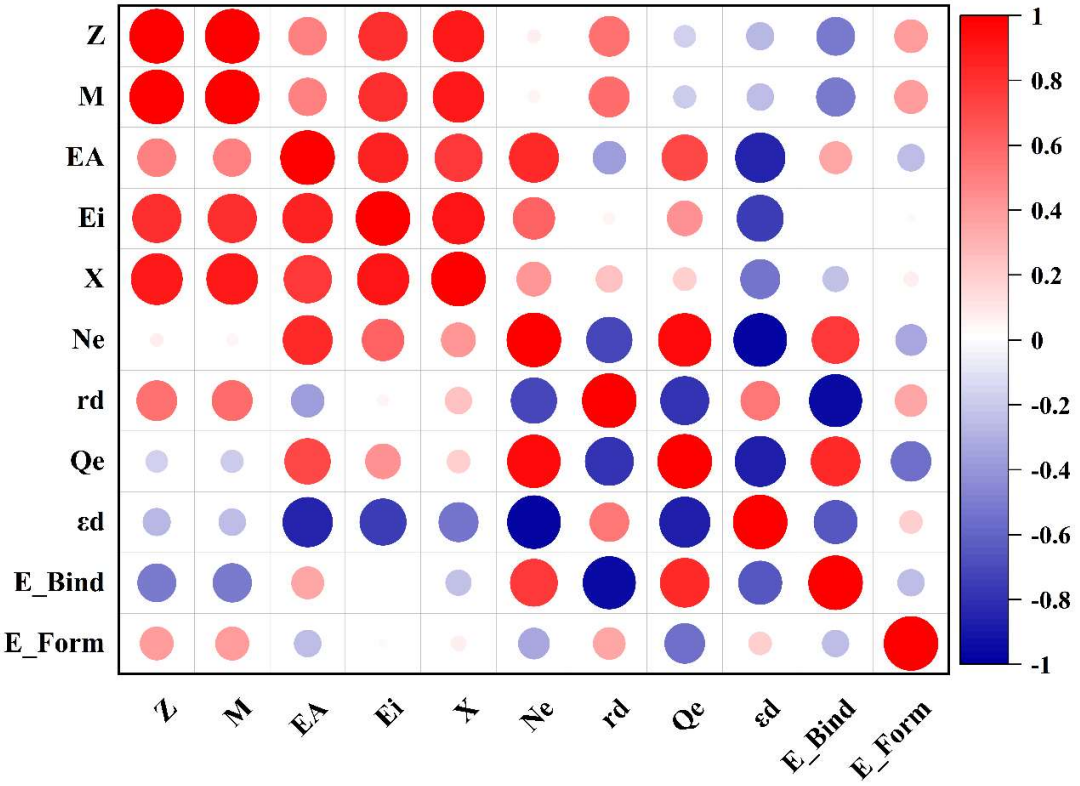

Figure S10. Pearson correlation of 11 feature variables. [Element (E), atomic number (Z), relative atomic mass (M), electron affinity (EA), first ionization energy (Ei), electronegativity (X), electron number of the d orbital (Ne), atomic radius (rd), charge transfer (Qe), d-band center (εd), binding energy (E_Bind), and formation energy (E_Form)].

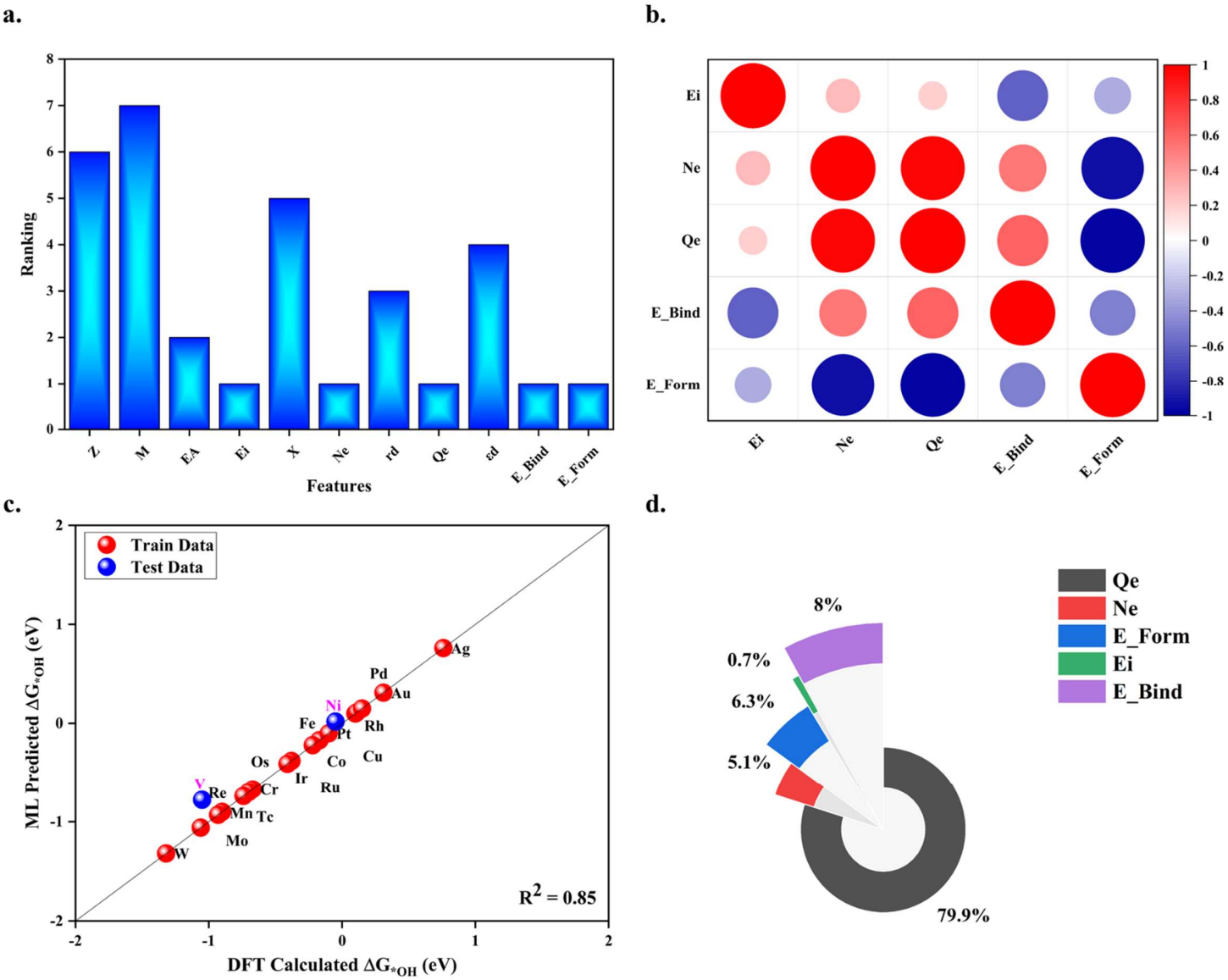

Figure S11. (a) The number of selected features *vs* features ranking. (b) Pearson correlation between selected features. (c) Calculated ΔG_{*OH} vs ML predicted ΔG_{*OH} by the GBR algorithm. (d) Feature importance of the GBR model for ΔG_{*OH}.

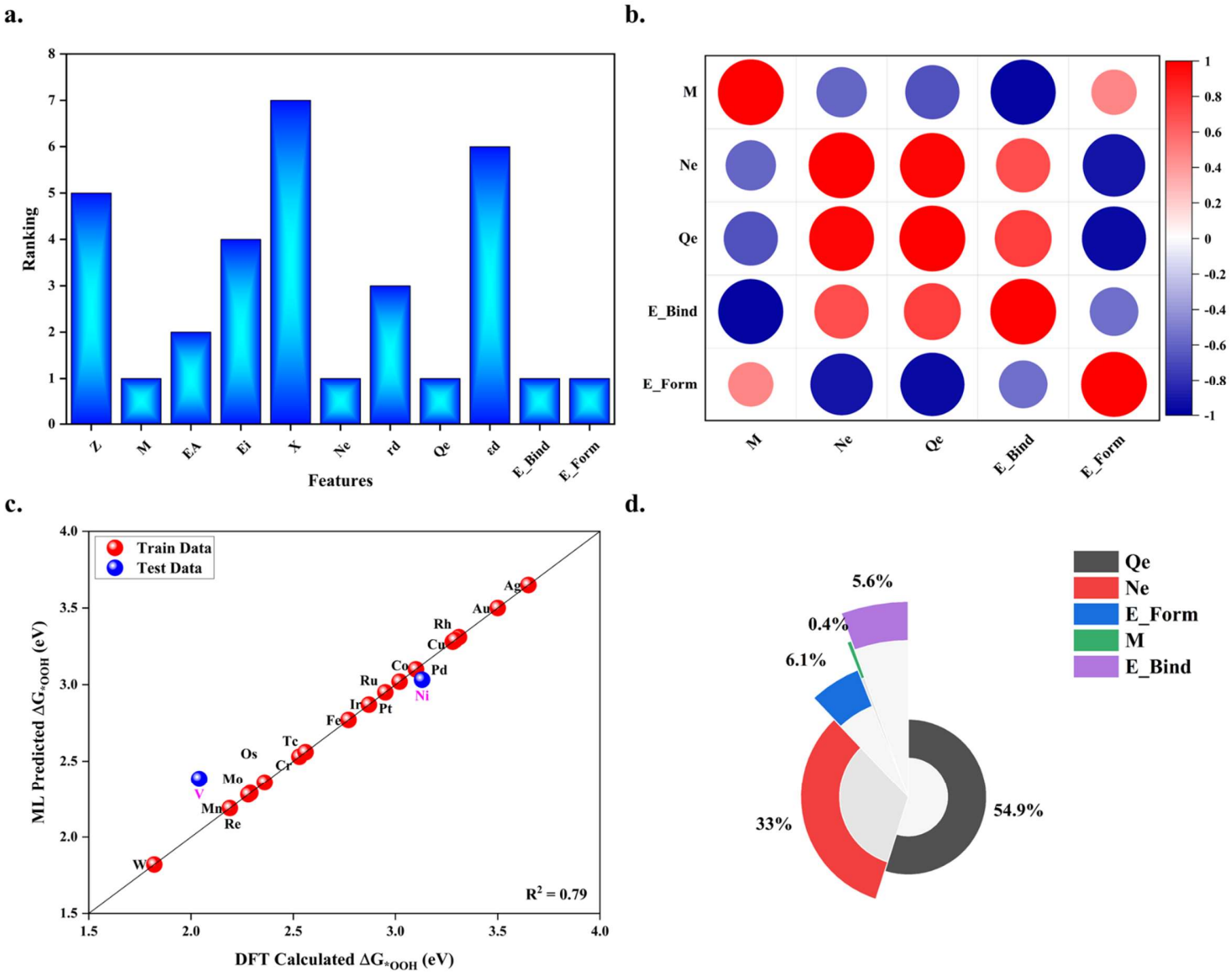

Figure S12. (a) The number of selected features *vs* features ranking. (b) Pearson correlation between selected features. (c) Calculated ΔG_{*OOH} vs ML predicted ΔG_{*OOH} by the GBR algorithm. (d) Feature importance of the GBR model for ΔG_{*OOH}.

Table S1. Adsorption energy of reaction intermediates using with and without dispersion correction on Pd@SV–BPN catalyst.

	G_{*H}	G_{*OH}	G_{*O}	G_{*OOH}
DFT	0.30	0.16	1.82	3.31
DFT-D3	0.26	0.16	1.82	3.31

Table S2. The defective C_1 and/or C_2 biphenylene vacancy formation energies (ΔE_{vf}) 2×2 and 3×3 unit cell.

surface	2X2	3X3
C_1-SV-BPN	5.029	4.714
C_2-SV-BPN	6.543	6.152

Table S3. The bond length between TM atom and SV-BPN substrate (d_{TM-d1}, d_{TM-d2}, d_{TM-d3} and d_{TM-d4}, with a unit of Å).

	d_{TM-d1}	d_{TM-d2}	d_{TM-d3}	d_{TM-d4}	Average
Sc	2.03	2.68 (/)	2.23	2.28	2.18 (2.08[11])
Ti	1.97	2.54 (/)	2.16	2.20	2.11 (1.93[12])
V	1.89	1.85	1.90	2.91 (/)	1.88 (1.88[11])
Cr	1.87	1.86	1.86	2.86 (/)	1.86 (1.85[11])
Mn	1.93	2.78 (/)	2.18	2.16	2.09 (1.83[11])
Fe	1.76	1.76	1.78	2.80 (/)	1.77 (1.76[11])
Co	1.76	1.78	1.78	2.77 (/)	1.77 (1.76[11])
Ni	1.78	1.87	1.79	2.70 (/)	1.81 (1.81[12])
Cu	1.90	2.79 (/)	2.20	2.12	2.07 (1.92[11])
Zn	2.03	3.00 (/)	2.63 (/)	2.64 (/)	
Y	2.15	2.74 (/)	2.36	2.42	2.31 (2.19[13])
Zr	2.09	2.69 (/)	2.21	2.33	2.21 (2.05[13])
Nb	2.00	2.27	2.23	2.87 (/)	2.0 (1.99[13])
Mo	1.98	1.95	1.97	2.96 (/)	1.96 (1.98[13])
Tc	1.91	1.90	1.93	2.93 (/)	1.91 (1.89[13])
Ru	1.88	1.89	1.90	2.89 (/)	1.89 (1.88[13])
Rh	1.88	1.93	1.90	2.84 (/)	1.90 (1.90[13])
Pd	1.92	2.02	1.92	2.78 (/)	1.95 (1.95[14])
Ag	2.11	3.19 (/)	2.89 (/)	2.85 (/)	2.11 (2.05[15])
Cd	2.32 (/)	3.40 (/)	3.13 (/)	3.10 (/)	
Hf	2.06	2.83 (/)	2.22	2.28	2.19 (2.02[16])
Ta	1.99	1.94	1.99	3.00 (/)	1.97 (1.96[16])
W	1.95	1.93	1.95	2.95 (/)	1.95 (1.94[16])
Re	1.91	1.91	1.92	2.93 (/)	1.92 (1.91[16])
Os	1.90	1.90	1.90	2.90 (/)	1.90 (1.89[16])
Ir	1.89	1.93	1.90	2.86 (/)	1.91 (1.90[16])
Pt	1.91	2.01	1.91	2.80 (/)	1.94 (1.94[11])
Au	1.98	3.21 (/)	3.07 (/)	3.11 (/)	1.98 (2.09[11])
Hg	3.53 (/)	3.82 (/)	3.68 (/)	3.84 (/)	

(/) represents there is no bond formation between TM and respected C (substrate) atoms.

Table S4. The formation (ΔE_{form}), binding energies (ΔE_{bind}) of TM atoms doped on SV@BPN, cohesive energies (ΔE_{coh}) of TM atoms in bulk, charge transfer (e^-) between TM atoms and SV@BPN and ε_d.

Catalysts	E_{form}	E_{bind}	E_{coh}	Charge (e^-)	ε_d
Sc@SV–BPN	-0.70	-4.80	-4.10	-1.92	0.70
Ti@SV–BPN	0.66	-4.57	-5.23	-1.71	-0.00
V@SV–BPN	-0.89	-6.09	-5.20	-1.75	-0.35
Cr@SV–BPN	-0.79	-4.86	-4.06	-1.42	-0.94
Mn@SV–BPN	0.78	-2.96	-3.74	-1.07	-2.69
Fe@SV–BPN	-0.90	-5.79	-4.89	-1.05	-1.55
Co@SV–BPN	-1.13	-6.29	-5.16	-0.75	-1.76
Ni@SV–BPN	-0.54	-5.51	-4.97	-0.73	-2.67
Cu@SV–BPN	0.76	-2.67	-3.43	-0.54	-2.37
Zn@SV–BPN	0.60	-0.59	-1.20	-0.45	-6.36
Y@SV–BPN	-0.65	-4.73	-4.07	-1.53	1.07
Zr@SV–BPN	0.74	-5.63	-6.36	-1.48	0.44
Nb@SV–BPN	2.20	-5.73	-7.93	-1.03	-0.38
Mo@SV–BPN	0.41	-5.95	-6.36	-2.27	-1.26
Tc@SV–BPN	0.08	-6.82	-6.90	-1.69	-1.60
Ru@SV–BPN	-0.72	-7.39	-6.67	-0.98	-1.71
Rh@SV–BPN	-1.14	-6.97	-5.83	-0.70	-2.63
Pd@SV–BPN	-0.14	-3.89	-3.75	-0.52	-4.04
Ag@SV–BPN	0.23	-1.67	-1.90	-0.33	-3.76
Cd@SV–BPN	0.35	-0.29	-0.65	-0.34	-7.82
Hf@SV–BPN	1.18	-5.59	-6.77	-2.56	0.09
Ta@SV–BPN	0.07	-8.00	-8.07	-3.15	-0.92
W@SV–BPN	1.19	-8.46	-9.65	-3.07	-1.38
Re@SV–BPN	1.01	-8.58	-9.58	-2.25	-1.56
Os@SV–BPN	0.24	-8.02	-8.26	-1.44	-1.75
Ir@SV–BPN	-0.62	-7.83	-7.21	-0.79	-2.75
Pt@SV–BPN	-0.36	-5.87	-5.51	-0.48	-4.06
Au@SV–BPN	0.07	-2.30	-2.36	-0.07	-3.25
Hg@SV–BPN	0.14	-0.02	-0.16	-0.01	-5.16

Table S5. The adsorption energy of ΔG_{*H} on TM@SV–BPN catalysts (unit in eV).

Catalyst	ΔG_{*H} (eV)	d_{TM-H} (Å)
Pt (111)	0.09	/
V@SV–BPN	0.14	1.68
Cr@SV–BPN	0.35	1.65
Mn@SV–BPN	-0.11	1.61
Fe@SV–BPN	0.16	1.54
Co@SV–BPN	0.45	1.56
Ni@SV–BPN	0.33	1.52
Cu@SV–BPN	0.48	1.51
Mo@SV–BPN	0.006	1.78
Tc@SV–BPN	-0.01	1.71
Ru@SV–BPN	0.17	1.67
Rh@SV–BPN	0.47	1.68
Pd@SV–BPN	0.30	1.65
Ag@SV–BPN	0.69	1.64
W@SV–BPN	-0.47	1.77
Re@SV–BPN	-0.51	1.73
Os@SV–BPN	-0.36	1.68
Ir@SV–BPN	-0.17	1.68
Pt@SV–BPN	-0.16	1.65
Au@SV–BPN	0.15	1.62

Table S6. The adsorption energies of *OH, *O and *OOH (ΔG_{*OH}, ΔG_{*O} and ΔG_{*OOH}) on TM@SV–BPN catalysts (unit in eV).

Catalysts	ΔG_{*OH} (eV)	ΔG_{*O} (eV)	ΔG_{*OOH} (eV)
V@SV–BPN	-1.04	-0.46	2.05
Cr@SV–BPN	-0.67	0.09	2.55
Mn@SV–BPN	-0.89	-0.04	2.21
Fe@SV–BPN	-0.38	0.72	2.79
Co@SV–BPN	-0.17	1.19	3.12
Ni@SV–BPN	-0.05	1.44	3.14
Cu@SV–BPN	0.10	2.25	3.30
Mo@SV–BPN	-0.93	-0.48	2.30
Tc@SV–BPN	-0.70	-0.40	2.58
Ru@SV–BPN	-0.21	0.91	2.97
Rh@SV–BPN	0.11	1.44	3.33
Pd@SV–BPN	0.16	1.82	3.31
Ag@SV–BPN	0.77	3.11	3.67
W@SV–BPN	-1.32	-1.18	1.84
Re@SV–BPN	-1.06	-0.77	2.30
Os@SV–BPN	-0.74	0.19	2.38
Ir@SV–BPN	-0.41	0.61	2.89
Pt@SV–BPN	-0.10	0.91	3.03
Au@SV–BPN	0.32	2.36	3.52

Table S7. The free energy change of each OER elementary step on TM@SV–BPN, described as ΔG_1, ΔG_2, ΔG_3 and ΔG_4, the ORR free energy change can be described as $-\Delta G_4$, $-\Delta G_3$, $-\Delta G_2$, and $-\Delta G_1$, unit of eV.

Catalysts	ΔG_1 (eV)	ΔG_2 (eV)	ΔG_3 (eV)	ΔG_4 (eV)	ΔG_5 (eV)	ΔG_6 (eV)	ΔG_7 (eV)	ΔG_8 (eV)
V@SV−BPN	-1.04	0.58	2.52	2.87	-2.87	-2.52	-0.58	1.04
Cr@SV−BPN	-0.67	0.76	2.46	2.37	-2.37	-2.46	-0.76	0.67
Mn@SV−BPN	-0.89	0.85	2.25	2.71	-2.71	-2.25	-0.85	0.89
Fe@SV−BPN	-0.38	1.10	2.07	2.13	-2.13	-2.07	-1.10	0.38
Co@SV−BPN	-0.17	1.36	1.93	1.80	-1.80	-1.93	-1.36	0.17
Ni@SV−BPN	-0.05	1.48	1.71	1.78	-1.78	-1.71	-1.48	0.05
Cu@SV−BPN	0.10	2.15	1.05	1.62	-1.62	-1.05	-2.15	-0.10
Mo@SV−BPN	-0.93	0.45	2.78	2.62	-2.62	-2.78	-0.45	0.93
Tc@SV−BPN	-0.70	0.30	2.98	2.34	-2.34	-2.98	-0.30	0.70
Ru@SV−BPN	-0.21	1.13	2.05	1.95	-1.95	-2.05	-1.13	0.21
Rh@SV−BPN	0.11	1.33	1.88	1.59	-1.59	-1.88	-1.33	-0.11
Pd@SV−BPN	0.16	1.66	1.49	1.61	-1.61	-1.49	-1.66	-0.16
Ag@SV−BPN	0.77	2.34	0.56	1.25	-1.25	-0.56	-2.34	-0.77
W@SV−BPN	-1.32	0.14	3.02	3.08	-3.08	-3.02	-0.14	1.32
Re@SV−BPN	-1.06	0.29	3.07	2.62	-2.62	-3.07	-0.29	1.06
Os@SV−BPN	-0.74	0.93	2.19	2.54	-2.54	-2.19	-0.93	0.74
Ir@SV−BPN	-0.41	1.02	2.27	2.03	-2.03	-2.27	-1.02	0.41
Pt@SV−BPN	-0.10	1.01	2.13	1.89	-1.89	-2.13	-1.01	0.10
Au@SV−BPN	0.32	2.04	1.16	1.40	-1.40	-1.16	-2.04	-0.32

Table S8. Theoretical over-potentials for OER (η^{OER}) and ORR (η^{ORR}) on TM@SV–BPN catalysts.

Catalysts	RDS		η^{OER} (V)	η^{ORR} (V)
	OER	ORR		
V@SV–BPN	ΔG_4	ΔG_8	1.64	2.27
Cr@SV–BPN	ΔG_3	ΔG_8	1.23	1.90
Mn@SV–BPN	ΔG_4	ΔG_8	1.48	2.12
Fe@SV–BPN	ΔG_4	ΔG_8	0.90	1.61
Co@SV–BPN	ΔG_3	ΔG_8	0.70	1.40
Ni@SV–BPN	ΔG_4	ΔG_8	0.55	1.28
Cu@SV–BPN	ΔG_2	ΔG_8	0.92	1.13
Mo@SV–BPN	ΔG_3	ΔG_8	1.55	2.16
Tc@SV–BPN	ΔG_3	ΔG_8	1.75	1.93
Ru@SV–BPN	ΔG_3	ΔG_8	0.82	1.44
Rh@SV–BPN	ΔG_3	ΔG_8	0.65	1.12
Pd@SV–BPN	ΔG_2	ΔG_8	0.43	1.07
Ag@SV–BPN	ΔG_2	ΔG_6	1.11	0.67
W@SV–BPN	ΔG_4	ΔG_8	1.79	2.55
Re@SV–BPN	ΔG_3	ΔG_8	1.84	2.29
Os@SV–BPN	ΔG_4	ΔG_8	1.31	1.97
Ir@SV–BPN	ΔG_3	ΔG_8	1.04	1.64
Pt@SV–BPN	ΔG_3	ΔG_8	0.90	1.33
Au@SV–BPN	ΔG_2	ΔG_8	0.81	0.91

Table S9. Computed results with solvent effect for OER/ORR on Co@, Rh@, and Ir@SV–BPN catalysts, unit eV.

Catalysts	ΔG_{*OH}	ΔG_{*O}	ΔG_{*OOH}	ΔG_1	ΔG_2	ΔG_3	ΔG_4	ΔG_5	ΔG_6	ΔG_7	ΔG_8	DFT-Sol		DFT		Difference	
												η^{OER}	η^{ORR}	η^{OER}	η^{ORR}	η^{OER}	η^{ORR}
Co@SV–BPN	-0.20	1.03	3.00	-0.20	1.23	1.98	1.92	-1.92	-1.98	-1.23	0.20	0.75	1.43	0.70	1.40	0.04	0.03
Rh@SV–BPN	0.08	1.32	3.21	0.08	1.24	1.90	1.71	-1.71	-1.90	-1.24	-0.08	0.67	1.15	0.65	1.12	0.01	0.03
Ir@SV–BPN	-0.48	0.41	2.74	-0.48	0.89	2.33	2.18	-2.18	-2.33	-0.89	0.48	1.10	1.71	1.04	1.64	0.06	0.08

Table S10. The magnetic moment (DFT and DFT+ U) with unit μ_B.

Catalysts	Magnetic		Catalysts	Magnetic		Catalysts	Magnetic	
	DFT	DFT+U		DFT	DFT+U		DFT	DFT+U
Sc@SV-BPN (U=2.90)	0.00	0.00	Y@SV-BPN	0.00	/	Hf@SV-BPN	0.00	/
Ti@SV-BPN ($U=4.40^{17}$)	0.90	1.87	Zr@SV-BPN	0.00	/	Ta@SV-BPN ($U=2.00^{17}$)	0.45	0.49
V@SV-BPN ($U=2.70^{17}$)	0.80	1.26	Nb@SV-BPN ($U=2.10^{17}$)	1.98	2.28	W@SV-BPN ($U=2.20^{17}$)	0.29	1.85
Cr@SV-BPN ($U=3.50^{17}$)	2.01	2.41	Mo@SV-BPN ($U=2.40^{17}$)	1.50	1.92	Re@SV-BPN ($U=2.40^{17}$)	0.97	0.97
Mn@SV-BPN ($U=4.00^{17}$)	3.62	4.51	Tc@SV-BPN ($U=2.70^{17}$)	1.02	1.83	Os@SV-BPN ($U=2.60^{17}$)	0.00	0.00
Fe@SV-BPN ($U=4.60^{17}$)	0.00	1.07	Ru@SV-BPN ($U=3.00^{17}$)	0.00	0.00	Ir@SV-BPN ($U=2.80^{17}$)	0.21	0.00
Co@SV-BPN ($U=5.00^{17}$)	0.02	0.00	Rh@SV-BPN ($U=3.30^{17}$)	0.12	0.00	Pt@SV-BPN ($U=3.00^{17}$)	0.00	0.00
Ni@SV-BPN ($U=5.10^{17}$)	0.00	0.00	Pd@SV-BPN ($U=3.60^{17}$)	0.00	0.00	Au@SV-BPN (U=4.00)	0.00	0.00
Cu@SV-BPN ($U=4.00^{17}$)	0.00	0.00	Ag@SV-BPN (U=5.80)	0.00	0.00	Hg@SV-BPN	0.84	/
Zn@SV-BPN ($U=7.50^{17}$)	0.45	0.41	Cd@SV-BPN ($U=2.10^{17}$)	0.46	0.46			

Table S11. Computed results of OER/ORR on selected catalysts (TM@SV–BPN). ΔG_{*OH}, ΔG_{*O}, ΔG_{*OOH}, ΔG_1, ΔG_2, ΔG_3, ΔG_4, ΔG_5, ΔG_6, ΔG_7, and ΔG_8, unit eV. η^{OER} and η^{ORR}, unit V.

Catalysts	ΔG_{*OH}	ΔG_{*O}	ΔG_{*OOH}	ΔG_1	ΔG_2	ΔG_3	ΔG_4	ΔG_5	ΔG_6	ΔG_7	ΔG_8	DFT + U		DFT		Difference	
												η^{OER}	η^{ORR}	η^{OER}	η^{ORR}	η^{OER}	η^{ORR}
V@SV-BPN	-1.02	-0.01	2.44	-1.02	1.00	2.45	2.48	-2.48	-2.45	-1.00	1.02	1.25	2.25	1.64	2.27	-0.39	-0.02
Cr@SV-BPN	-0.43	1.04	2.82	-0.43	1.47	1.78	2.10	-2.10	-1.78	-1.47	0.43	0.87	1.66	1.23	1.90	-0.36	-0.24
Mn@SV-BPN	-0.78	1.00	2.62	-0.78	1.78	1.62	2.30	-2.30	-1.62	-1.78	0.78	1.07	2.01	1.48	2.12	-0.41	-0.11
Fe@SV-BPN	0.00	1.02	3.31	0.00	1.03	2.29	1.61	-1.61	-2.29	-1.03	0.00	1.06	1.23	0.90	1.61	0.16	-0.38
Co@SV-BPN	0.02	1.53	3.33	0.02	1.51	1.81	1.59	-1.59	-1.81	-1.51	-0.02	0.58	1.21	0.70	1.40	-0.12	-0.19
Ni@SV-BPN	0.02	1.72	3.19	0.02	1.69	1.47	1.73	-1.73	-1.47	-1.69	-0.02	0.50	1.21	0.55	1.28	-0.05	-0.07
Cu@SV-BPN	0.32	2.51	3.44	0.32	2.20	0.93	1.48	-1.48	-0.93	-2.20	-0.32	0.97	0.91	0.92	1.13	0.05	-0.22
Mo@SV-BPN	-0.90	-0.19	2.51	-0.90	0.71	2.70	2.41	-2.41	-2.70	-0.71	0.90	1.47	2.13	1.55	2.16	-0.08	-0.03
Tc@SV-BPN	-0.64	0.01	2.64	-0.64	0.65	2.63	2.28	-2.28	-2.63	-0.65	0.64	1.40	1.87	1.75	1.93	-0.35	-0.06
Ru@SV-BPN	-0.16	1.00	2.99	-0.16	1.17	1.98	1.93	-1.93	-1.98	-1.17	0.16	0.75	1.39	0.82	1.44	-0.07	-0.05
Rh@SV-BPN	0.38	1.70	3.55	0.38	1.33	1.84	1.37	-1.37	-1.84	-1.33	-0.38	0.61	0.85	0.65	1.12	-0.04	-0.27
Pd@SV-BPN	0.32	2.17	3.44	0.32	1.85	1.27	1.48	-1.48	-1.27	-1.85	-0.32	0.62	0.91	0.43	1.07	0.19	-0.16
Ag@SV-BPN	1.05	3.50	3.84	1.05	2.45	0.34	1.08	-1.08	-0.34	-2.45	-1.05	1.22	0.89	1.11	0.67	0.11	0.22
Ir@SV-BPN	-0.19	0.85	3.08	-0.19	1.03	2.23	1.84	-1.84	-2.23	-1.03	0.19	1.00	1.42	1.04	1.64	-0.04	-0.22
Pt@SV-BPN	0.08	1.20	3.13	0.08	1.12	1.93	1.79	-1.79	-1.93	-1.12	-0.08	0.70	1.15	0.90	1.33	-0.20	-0.18
Au@SV-BPN	0.55	2.69	3.67	0.55	2.14	0.98	1.25	-1.25	-0.98	-2.14	-0.55	0.91	0.68	0.81	0.91	0.10	-0.23

Table S12. Bifunctional over-potential for water-splitting (W–η^{Bi}) and metal-air batteries (M–η^{Bi}), unit in V.

Catalysts	η^{HER}	η^{OER}	η^{ORR}	W–η^{Bi}	M–η^{Bi}
V@SV–BPN	0.14	1.64	2.27	1.78	3.91
Cr@SV–BPN	0.35	1.23	1.90	1.58	3.13
Mn@SV–BPN	0.11	1.48	2.12	1.59	3.60
Fe@SV–BPN	0.16	0.90	1.61	1.06	2.51
Co@SV–BPN	0.45	0.70	1.40	1.15	2.10
Ni@SV–BPN	0.33	0.55	1.28	0.87	1.82
Cu@SV–BPN	0.48	0.92	1.13	1.40	2.04
Mo@SV–BPN	0.006	1.55	2.16	1.56	3.71
Tc@SV–BPN	0.01	1.75	1.93	1.76	3.68
Ru@SV–BPN	0.17	0.82	1.44	0.99	2.27
Rh@SV–BPN	0.47	0.65	1.12	1.12	1.77
Pd@SV–BPN	0.30	0.43	1.07	0.73	1.50
Ag@SV–BPN	0.69	1.11	0.67	1.81	1.79
W@SV–BPN	0.47	1.79	2.55	2.25	4.33
Re@SV–BPN	0.51	1.84	2.29	2.34	4.13
Os@SV–BPN	0.36	1.31	1.97	1.67	3.28
Ir@SV–BPN	0.17	1.04	1.64	1.21	2.68
Pt@SV–BPN	0.16	0.90	1.33	1.05	2.22
Au@SV–BPN	0.15	0.81	0.91	0.97	1.72

Table S13. Element (*E*), atomic number (*Z*), relative atomic mass (*M*), electron affinity (*EA*), first ionization energy (*E*i), electronegativity (*X*), electron number of the d orbital (*Ne*), atomic radius (rd), charge transfer (*Qe*), d-band center (ε_d), binding energy (E_{bind}), and formation energy (E_{form}).

E	*Z*	*M*	*EA*	*Ei*	*X*	*Ne*	*rd*	*Qe*	ε_d	E_{Bind}	E_{Form}
V	23	51	0.524	6.746	1.63	3	1.79	-1.75	-0.35	-6.09	-0.89
Cr	24	52	0.666	6.767	1.66	5	1.89	-1.41	-0.93	-4.86	-0.79
Mn	25	55	0	7.434	1.55	5	1.97	-1.06	-2.68	-2.96	0.78
Fe	26	56	0.163	7.903	1.83	6	1.94	-1.05	-1.55	-5.79	-0.9
Co	27	59	0.66	7.881	1.88	7	1.92	-0.75	-1.75	-6.29	-1.13
Ni	28	59	1.16	7.64	1.91	8	1.63	-0.73	-2.66	-5.51	-0.54
Cu	29	64	1.227	7.727	1.9	10	1.4	-0.54	-2.36	-2.67	0.76
Mo	42	96	0.745	7.092	2.16	5	2.09	-2.26	-1.26	-5.95	0.41
Tc	43	98	0.55	7.28	1.9	5	2.09	-1.69	-1.59	-6.82	0.08
Ru	44	101	1.05	7.361	2.2	7	2.07	-0.97	-1.71	-7.39	-0.71
Rh	45	103	1.137	7.459	2.28	8	1.95	-0.7	-2.63	-6.97	-1.14
Pd	46	106	0.557	8.337	2.2	10	2.02	-0.51	-4.04	-3.89	-0.14
Ag	47	108	1.302	7.576	1.93	10	1.72	-0.32	-3.76	-1.67	0.23
W	74	184	0.815	7.98	2.36	4	2.1	-3.07	-1.37	-8.46	1.19
Re	75	186	0.15	7.88	1.9	5	2.17	-2.25	-1.55	-8.57	1
Os	76	190	1.1	8.71	2.2	6	2.16	-1.43	-1.75	-8.02	0.24
Ir	77	192	1.57	9.12	2.2	7	2.02	-0.79	-2.75	-7.82	-0.62
Pt	78	195	2.128	9.02	2.28	9	2.09	-0.48	-4.05	-5.87	-0.36
Au	79	197	2.309	9.225	2.54	10	1.66	-0.07	-3.25	-2.29	0.07

Table S14. Evaluated R^2, MAE, and RMSE metrics to predict ΔG_{*OH}, ΔG_{*O} and ΔG_{*OOH} for test and train data.

		R^2	MAE	RMSE
ΔG_{*OH}	Test	1.00	0.00	0.00
	Train	0.85	0.17	0.20
ΔG_{*O}	Test	1.00	0.00	0.00
	Train	0.99	0.10	0.12
ΔG_{*OOH}	Test	1.00	0.00	0.00
	Train	0.79	0.22	0.25

Reference:

1. J. K. Nørskov, J. Rossmeisl, A. Logadottir, L. Lindqvist, J. R. Kitchin, T. Bligaard and H. Jonsson, *J. Phys. Chem. B*, 2004, **108**, 17886-17892.
2. , DOI: http://cccbdb.nist.gov/.
3. V. Wang, N. Xu, J.-C. Liu, G. Tang and W.-T. Geng, *Comput. Phys. Commun.*, 2021, **267**, 108033.
4. J. K. Nørskov, T. Bligaard, A. Logadottir, J. Kitchin, J. G. Chen, S. Pandelov and U. Stimming, *J. Electrochem. Soc.*, 2005, **152**, J23.
5. G. W. Watson, R. P. Wells, D. J. Willock and G. J. Hutchings, *J. Phys. Chem. B*, 2001, **105**, 4889-4894.
6. D. Zhan, J. Velmurugan and M. V. Mirkin, *Journal of the American Chemical Society*, 2009, **131**, 14756-14760.
7. G. J. Kubas, *Journal of Organometallic Chemistry*, 2001, **635**, 37-68.
8. S.-J. Woo, E.-S. Lee, M. Yoon and Y.-H. Kim, *Phys. Rev. Lett.*, 2013, **111**, 066102.
9. J. Rossmeisl, Z.-W. Qu, H. Zhu, G.-J. Kroes and J. K. Nørskov, *J. Electroanal. Chem.*, 2007, **607**, 83-89.
10. G. Gao, E. R. Waclawik and A. Du, *J. Catal.*, 2017, **352**, 579-585.
11. A. Krasheninnikov, P. Lehtinen, A. S. Foster, P. Pyykkö and R. M. Nieminen, *Phys. Rev. Lett.*, 2009, **102**, 126807.
12. C. Ramos-Castillo, J. Reveles, M. Cifuentes-Quintal, R. Zope and R. De Coss, *J. Phys. Chem. C*, 2016, **120**, 5001-5009.
13. M. Sun, Q. Ren, Y. Zhao, J.-P. Chou, J. Yu and W. Tang, *Carbon*, 2017, **120**, 265-273.
14. Q. Luo, W. Zhang, C.-F. Fu and J. Yang, *International Journal of Hydrogen Energy*, 2018, **43**, 6997-7006.
15. X. Zhang, R. Huang, Y. Gui and H. Zeng, *Sensors*, 2016, **16**, 1830.
16. M. Sun, W. Tang, Q. Ren, Y. Zhao, S. Wang, J. Yu, Y. Du and Y. Hao, *Physica E Low Dimens. Syst. Nanostruct.*, 2016, **80**, 142-148.
17. W. Setyawan, R. M. Gaume, S. Lam, R. S. Feigelson and S. Curtarolo, *ACS combinatorial science*, 2011, **13**, 382-390.